DiVA
http://www.diva-portal.org

Postprint

This is the accepted version of a paper published in *Journal of nanoparticle research*. This paper has been peer-reviewed but does not include the final publisher proof-corrections or journal pagination.

Citation for the original published paper (version of record):

Hedayati, M., Sharma, P., Katyal, D., Fagerlund, F. (2016)
Transport and retention of carbon-based engineered and natural nanoparticles through saturated porous media.
Journal of nanoparticle research, (70)
http://dx.doi.org/10.1007/s11051-016-3365-6

Access to the published version may require subscription.

N.B. When citing this work, cite the original published paper.

Accepterad version

Permanent link to this version:
http://urn.kb.se/resolve?urn=urn:nbn:se:uu:diva-292975

Abstract

Carbon–based engineered nanoparticles have been widely used due to their small size and unique physical and chemical properties. At the same time, the toxic effect of these nanoparticles on human and fish cells has also been observed; therefore, their release and distribution into the surface and subsurface environment is a subject of concern. The aim of this research is to evaluate and compare transport and retention of two types of engineered nanoparticles (multi-walled carbon nanotubes (MWCNT) and C_{60}) and natural carbon nanoparticles collected from a fire accident. Several laboratory experiments were conducted to observe transport behavior of nanoparticles through a column packed with silica sand. The column experiments were intended to monitor the effect of ionic strength on transport of nanoparticles as a function of their shapes. It was observed that the mobility of both types of engineered nanoparticles was reduced with increase in ionic strength from 1.34 mM to 60 mM. However, at ionic strength upto 10.89 mM, spherical nanoparticles were more mobile than cylindrical nanoparticles but the mobility of cylindrical nanoparticles became significantly higher than spherical nanoparticles at 60 mM. In comparison with natural fire nanoparticles, both types of engineered nanoparticles were much less mobile at the selected experimental condition in this study. Furthermore, inverse modeling was used to calculate parameters such as attachment efficiency, the longitudinal dispersivity, and capacity of the solid phase for the attachment of nanoparticles. The results indicate that the combination of nanoparticles shape and their solution chemistry are responsible for the transport and retention of nanoparticles in natural environment however fire burned particles can be highly mobile at the natural groundwater chemistry.

Keywords: Carbon-based nanoparticles; transport; retention; porous media; modeling.

1. Introduction

The last decade has seen growth of nanotechnology into a prominent, interdisciplinary field that influences almost every major branch of science. Engineered nanoparticles (ENPs) constitute the fundamental building blocks in nano-technological applications and are compositionally categorized as carbonaceous (e.g., carbon black, fullerene (C_{60}), carbon nanotubes (CNTs)) and non-carbonaceous (e.g., oxide nanoparticles like TiO_2, ZnO, SiO_2 and quantum dots, dendrimers). Carbon-based nanoparticles have been the focus of much interest due to their unique physical and chemical properties. They have been proposed for many applications and implemented in various fields, such as nonlinear optical material (Wang et al., 2009), medical devices and pharmaceuticals (He et al., 2013), energy conversion, environmental monitoring and waste water treatments (Tan et al., 2012) and in lots of consumer products (Grassian, 2008). Because of the extensive usage, their production and disposal are expected to increase dramatically over the next several decades (Klaine et al., 2008).

Concerns over the potential adverse effects of exposure to carbon based nanoparticles (such as, nano C_{60} and CNTs) have initiated research on their fate and transport in the environment (Petersen et al., 2011). Although allotropes of carbon, fullerene (C_{60}) and CNTs are hydrophobic in nature, the dispersion of multi-walled carbon nanotubes (MWNTs) and C_{60} into water in the presence of natural organic matter (NOM) has been reported recently (Hyung et al., 2007; Mashayekhi et al., 2012; Zhang et al., 2014). Natural carbon-based nanoparticles can also be formed during the incomplete burning of coal, oil and gas, garbage or other organic substances (Nisbet and LaGoy, 1992). Migration of these particles, which typically contain large amounts of metals and poly-aromatic hydrocarbons (PAH), is a subject of concern (Hertzberg and Blomqvist, 2003; Sharma et al., 2016).

Chemical and physical conditions of the environment can affect mobilization of carbon based nanoparticles through porous media. Previous studies have investigated the effect of chemistry of the solution, water content, porous media grain size (Sharma et al., 2014; Mattison et al., 2011), degree of saturation (Mekonen et al., 2014), flow rate (Liu et al., 2009), concentration (Kasel et al., 2013) and the particle diameter (O'Carroll et al., 2013). However, the effect of shape of carbon based nanoparticles on their transport and retention is still scarcely reported (Seymour et al., 2013).

A spherical (C60), a cylindrical (CNT), and natural (fire born) nanoparticles are chosen in this study. Although the toxicity of C_{60} nanoparticles and carbon nanotubes (CNTs) in aqueous suspensions has been studied, the current understanding of their fate and transport in subsurface environments is quite limited. Furthermore, no comparative evaluation of the fate of C_{60}, CNTs and other natural carbon particles (such as fire born particles (FBP)) has been reported in literature. This study proposes to fill this gap by comparing the effect of ionic strength on the transport and mobilization behavior of these three distinguished shape of carbon-based nanoparticles in saturated porous media by conducting a series of laboratory column experiments. A 1-D finite element model was also used to simulate the experiments, examine the ability of the model to capture the observed particle retention and find unknown transport parameters such as dispersivity, attachment efficiency and maximum adsorption capacity. Derjaguin-Landau-Verwey-Overbeak (DLVO) theory was employed to understand the effective mechanisms responsible for retention of these nanoparticles.

2. Material and methods

2.1. Nanoparticles

2.1.1. C_{60}: A stable aqueous solution of spherical C_{60} was prepared by using the method proposed by Brant et al (2006). In brief, 20 gm of fullerene (C_{60}, sublimed 99%) powder procured from Sigma-Aldrich was dissolved in 20 ml of toluene then the solution was diluted

by addition of 200 ml of de-ionized (DI) water and sonicated for 1.5 hours using ultra-probe sonicator (ultrasonic homogenizer, Biologics Inc., Model 3000) with 40% power output, followed by 1 h sonication using bath sonicator in order to disperse the nanoparticles in the solution (Kerry Ultrasonic LTD, 50 Hz). The large aggregations were then filtered through 11-μm nylon filter membrane (Nylon Net Filter, Merck Millipore Ltd, NY1100010, MA, USA). The final concentration of C_{60} solution was 7 mg/l for column experiments. The zeta potential and hydrodynamic diameters of C_{60} solution at their respective ionic strength were measured using zeta sizer (Malvern Instruments). A 24 h test to check the stability of the particles resulted in no change in concentration during the experimental period.

2.1.2. Multi-walled carbon nanotubes: Multi-walled carbon nanotubes (MWCNTs) (95% pure) with diameters 20-30 nm and length 0.5-2 μm were purchased from Cheap Tubes, Inc (Brattleboro, USA). In order to dissolve MWCNTs in aqueous solution for column experiments, functionalization using concentrated sulfuric/nitric acid in the ratio of 3:1 was performed (Liu et al., 1998; Sharma and Fagerlund 2014; Mekonen et al., 2014). Finally, the solution was filtered through 11-μm hydrophilic nylon filter membrane (Nylon Net Filter, Merck Millipore Ltd, NY1100010, MA, USA) and washed with hot Deionized water (DI water). The functionalized MWCNTs were finally diluted to a concentration of 7 mg/L with DI water and sonicated for 30 minutes using the ultra-probe sonicator (ultrasonic homogenizer, Biologics Inc., Model 3000). The zeta potential and hydrodynamic diameters of MWCNT solution at their respective ionic strength were measured using zeta sizer.

2.1.3. Fire born particles: A sample in aqueous phase was collected from a fire location, which was filtered with 11-μm nylon filter. SEM images of the sample revealed that the average size of irregular shaped particles was 200±5 nm, however, the hydrodynamic diameter of the filtered FBP stock solution were measured using zeta sizer. Chemical analysis of this sample reflected the presence of PAH (Sharma et al., 2016). The ionic strength of the

sample was estimated to be around 60 mM using eq 1, from its measured electrical conductivity value (Lind, 1970):

$$I_c = (1.4769 \times 10^{-5}) \times (EC) + 0.00015 \quad (1)$$

where I_c is ionic strength (M), EC is electrical conductivity (μS/cm). The pH of the sample was adjusted to 7 by addition of HCl acid to match the chemistry of the other two nanoparticles.

2.2. Porous media

The silica sand was purchased from Sibelco Nordic, Baskarp, Sweden to be used as porous media in the column experiment after sieving by 250 and 400 μm sieves. The sand was washed with hydrochloric acid (0.1 M) and hydrogen peroxide (7%) according to the method of Sharma and Fagerlund (2014) to remove impurities. Finally the sand was washed several times with DI water. The washed sand was dried in the oven at 105°C for 24 hours and stored in a plastic bottle. The surface potential of the sand at different ionic strength and the selected pH are determined using SurPASS Electrokinetic Analyzer (Anton Paar USA Inc., Ashland, VA).

2.3. Column experiments

A borosilicate glass column (Chormaflex Inc.) with two steel mesh filters (0.2 mm) combined with 100 μm nylon filters at each end was used for the column experiments. The size of the column chosen in this study was 15 cm length and 2.5 cm diameter, the length and diameter ratio of the column for the selected porous media was adequate to avoid the preferencial flow along the wall (Arbuckle and Ho, 1990). The column was packed with 120 g silica sand and flushed with background solution which was buffered to pH 7 with sodium phosphate buffer. The properties of the sand filled column are listed in Table 1. A calibrated peristaltic pump (IPC8, Ismatic, Glattbrug, Switzerland) was used to inject the experimental solutions into the sand column. These experimental solutions were aqueous suspension of C_{60}, MWCNT and

FBP with the same pH and ionic strength as the background solution. The experiments were started (at time zero) by injecting the main solution to the column for about five pore volumes of experimental solution (C_{60}, MWCNT or FBP) (Phase I) followed by three pore volumes of background solution (Phase II). Thereafter, three pore volume of DI water was introduced into the column (phase III) to investigate the remobilization of the retained particles. The effluent solution was directed to a UV/vis Spectrophotometer (Model DR 5000, Hach Lange Ltd) in order to measure the absorbance/concentration of the outflow sample at an interval of 1 min using an auto sampler at a fixed wavelength (344 nm for C60, 332 nm for MWCNT, and 400 nm for FBP). The effluent fractions were also collected at 5 min interval using fraction collector (CF-2, Spectrum Labs Inc.). To assess the water flow and hydrodynamic dispersion in the column, a tracer test with a 2 mM sodium chloride solution was conducted. Five pore volumes of tracer solution were injected followed by three pore volume of DI-water. All other parameters were kept constant throughout these experiments (i.e. porous media characteristics, temperature, flow rate and pH) while the ionic strength was varied from 1.34 to 60 mM. All experiments are performed in triplicate and the experimental protocols are summarized in Table 2.

2.4. DLVO theory

Derjaguin-Landau-Verwey-Overbeak (DLVO) theory is the most common theory that has been used to explain aggregation, transport and retention of nanoparticles under different chemical conditions (Sharma et al., 2008a; 2008b; 2014; Jiang et al., 2009; Kasel et al., 2013; Mekonen et al., 2014). Based on DLVO theory, sum of van der Waals attractive energy (E_V) and electrostatic double layer energy (E_{edl}) controls the interaction between particles and the resulting net energies (the interaction energy (E_i)) can be used to predict the probability of particle attachment (Wang et al., 2008; Sharma et al., 2008c). Particles can have a net attraction in a primary or secondary minimum. Aggregation at the primary minimum is

irreversible but there is a possibility of attachment of a particle at secondary minimum only at a particular separation distance. E_v and E_{edl} can be calculated using following equations (Gregory, 1981):

$$E_v = -\frac{Aa}{12d}\left[1 - \frac{5.32d}{\lambda}\ln\left(1 + \frac{\lambda}{5.32d}\right)\right] \quad (2)$$

$$E_{edl} = \frac{64\pi nkTa}{\kappa^2} tanh^2\left(\frac{ze\zeta}{4kT}\right) e^{(-\kappa d)} \quad (3)$$

where, A is Hamaker constant (6.7×10^{-21} J for C_{60} (Chen and Elimelech, 2006), 9.8×10^{-21} J for MWCNTs (Mekonen et al., 2014) and 3.84×10^{-21} J for FBP (Sharma et al., 2016). λ is the characteristic wavelength of the interaction, which is assumed to be 100 nm, a is the particle radius and d is the separation distance (m), k is the Boltzmann constant ($1.38.10^{-23}$ J/K), T is the absolute temperature (K), z is the ion valence (-), e is the electron charge (1.6×10^{-19} coulombs), and ζ is the surface potential of particles and the sediments (the surface potential can be approximated by the determination of zeta potential) (Sharma et al., 2008c).

If ε_r is the relative dielectric constant of water (78.55) and ε_0 is the vacuum permittivity constant, the inverse of Debye-Huckel length 'κ' can be calculated from the following formula:

$$\kappa = \sqrt{\frac{2e^2 N_A\ I_c}{\varepsilon_r\ \varepsilon_0 kT}} \quad (4)$$

where N_A is the Avogadro number and I_c is the ionic strength of the solution (Wang et al., 2008). To calculate the interaction energy between MWCNTs and porous media, hydrodynamic diameter was used as their effective size (Tian et al., 2012).

2.5. Mathematical model

A numerical model (1-D finite element code) was used to simulate the transport of C_{60}, MWCNT, and FBP in porous media (Liu et al., 2009). The model is based on mass balance in the aqueous solution (eq 5) and solid phases (eq 6):

$$\frac{\partial C}{\partial t} + \frac{\rho_b}{n}\frac{\partial S}{\partial t} + v\frac{\partial C}{\partial x} - D\frac{\partial^2 C}{\partial x^2} = 0 \quad (5)$$

$$\frac{\rho_b}{n}\frac{\partial S}{\partial t} - k_{att}\psi C + \frac{\rho_b k_{det}}{n} S = 0 \quad (6)$$

where C is the concentration of nanoparticle in the aqueous phase, t is time, ρ_b is the solid phase bulk density, n is porosity, S is the amount of particles associated with the solid phase, v is the pore water velocity, x is the spatial dimension in the column and D is the dispersion coefficient ($D = v * \alpha_L$, where α_L is the longitudinal dispersivity). k_{att} is the attachment coefficient associated with mechanisms typically linked with colloid filtration theory (Liu et al., 2009). ψ is an attachment site blocking term and k_{det} is the rate constant for the detachment of nanoparticles associated with the solid phase. The attachment site blocking term is defined as:

$$\psi = 1 - \frac{S}{S_{max}} \quad (7)$$

where S_{max} is the maximum adsorption capacity of the solid phase for the attachment of particles due to mechanisms typically associated with colloid filtration theory, the attachment rate constant k_{att} is defined as:

$$k_{att} = \frac{3\alpha\eta_0 v(1-n)}{2d_c} \quad (8)$$

where α is the attachment efficiency, η_0 is the total single collector efficiency and d_c is the mean diameter of the collector (sand grain). The attachment efficiency (α) typically fits to the experimental data whereas the total single collector efficiency is based on theoretical considerations.

The total collector efficiency (η_0) is assumed to be the sum of three distinct collision mechanisms, collision due to particle interception (η_I), gravity sedimentation (η_G), and diffusion (η_D) (Sharma et al., 2008a; Liu et al., 2009; Sharma 2012). In order to estimate the unknown parameters, the model was programmed to find the best set of parameters which produce the simulated breakthrough curve with minimum root-mean-square error (RMSE) from the observed breakthrough curve using an optimization routine.

196 **3. Results**

197 **3.1. Experiments**

198 Experimental results from sand-packed columns and dispersed aqueous suspensions of the
199 nanoparticles (pH=7) at different ionic strengths ranging from 1.34 mM to 60 mM are shown
200 in Fig 1. The response of spherical nanoparticles (C_{60}) and cylindrical nanoparticles
201 (MWCNT) breakthrough curves with increasing ionic strength was in same order and the
202 retention of both nanoparticles were enhanced with increase in ionic strength, which is
203 consistent with previous studies (Brant et al. 2005; Zhang et al., 2012; Sharma et al., 2014).
204 The concentration of nanoparticles in the effluent increased rapidly initially, and then the
205 relative concentration increased at a much lower rate in phase I. As background solution was
206 injected into the column during phase II, the concentration of nanoparticles decreased and
207 reached close to zero. The shape of the breakthrough curves (BTCs) was also more
208 asymmetric at elevated ionic strength, and the rate of increase in relative concentration was
209 faster (steeper slope) for MWCNTs than for C_{60}. As the concentration of salt in the
210 suspension increased, the difference between the breakthrough curves for MWCNTs and C_{60}
211 became larger (Fig 1). At ionic strength 1.34 mM and 10.89 mM, the breakthrough curves for
212 both types of nanoparticles were less variable even though the C_{60} particles were relatively
213 more mobile than MWCNTs. The maximum relative concentration of both C_{60} and
214 MWCNTs in the effluent was 0.93 at ionic strength of 1.34 mM at 5.67 pore volume (PV) but
215 slightly higher mobility was observed for C_{60} nanoparticles as ionic strength increased to
216 10.89 mM. However, at the highest ionic strength (60 mM), MWCNTs became more mobile
217 than C_{60}, and the relative concentration of MWCNTs in the effluent reached a maximum
218 value of 0.69 while the corresponding maximum value was 0.4 for C_{60} particles (Fig 1). In
219 Section 3.3, the attachment term through numerical modeling for both cases has been
220 discussed. The area under the BTCs was calculated and considered as the total mass of the

nanoparticles in the effluent for all the experiments, as shown in Fig 2a. Only 12% of the total injected MWCNTs and 10% of C_{60} nanoparticles were retained in the column at ionic strength 1.34 mM, while at an ionic strength of 60 mM about 40% of the MWCNTs and 68% of the C_{60} were trapped in the porous medium (Fig 2a).

A column experiment was performed to investigate the transport of FBP at ionic strength 60 mM and pH 7 (at their original solution chemistry), which is shown in Fig 3. The BTC shape was asymmetric; the maximum relative concentration of FBP in the effluent was 0.92 which was achieved at 5.7 PV. After 11 PVs (phase I, II and III) 90% of the injected mass was recovered in the effluent. The image analysis (using Scanning Electron Microscope) indicates that the particle sizes of FBP in the influent and effluent samples were in the same order of magnitude (Fig 4).

3.2. Remobilization

The mechanisms responsible for retention and transport of nanoparticles at different chemical conditions in the experiments were investigated using DLVO energy profiles. The zeta potential and hydrodynamic diameters of C_{60} solution at their respective ionic strength and the average diameter of the nanoparticles in stock solution are shown in Table 3. The role of secondary energy minima in retention of the particles in the sand column at different ionic strengths was investigated by injecting DI water into the column during phase III. All BTCs of the experimental data (MWCNT, C_{60} and FBP experiments) showed a secondary peak at 9.2 pore volumes which is 1.2 PV after injection of DI water into the column and the peak height raised with increasing ionic strength (Phase III of Fig 2b for C_{60} and MWCNT respectively but FBP data not presented in this paper). Mass calculations indicated that at low ionic strength (1.34 mM), 7% of the total injected MWCNTs and C_{60} were remobilized during phase III. This percentage increased to 40.3% for C_{60} and 28.9% for MWCNTs at high

ionic strength (60 mM) (Fig 2b). It was observed that only 12.32% of the retained FBP were remobilized during phase III (data not presented in the paper).

The DLVO energy profiles for both C_{60} and MWCNTs indicated that a reduction in primary energy height and increase in secondary energy minimum with increase in ionic strength (Fig 5). However, the separation distance for primary energy minimum reduces with increase in ionic strength, i.e., the nanoparticles need to stay more closer to the sand surfaces for primary minimum attachment for high ionic strength condition (but opposite for possible attachment at the secondary minimum).

3.3. Modeling

The model, which incorporates traditional colloid filtration theory with a site-blocking term and a detachment rate, was in a good agreement with the experimental results (Fig 1 & 3). The observed data of all column experiments were used in the inverse modelling to simulate breakthrough curves of MWCNTs, C_{60} and FBP and find the best set of unknown transport parameters. The fitted dispersivity with the observed BTC of the tracer experiment was 0.0026 m. Since dispersivity is a medium dependent parameter (Xu and Eckstein, 1997), this value was kept constant for the rest of the simulations. The calculation of theoretical single collector efficiency (η) for MWCNTs, tested under assumption of both end contact and side contact (as similar to Liu et al., 2009), revealed that diffusion, which is independent of orientation (Wang et al., 2008), is the dominant mechanism for transport of particles to the surfaces of sand. Thus, it was assumed that the attachment of MWCNTs was possibly through side contact with the collector. Similar calculations for C_{60} particles also confirmed that the dominant mechanism is diffusion (99.7%). To calculate the theoretical single collector efficiency for FBP, it was assumed that the particles are spherical in shape (based on SEM images in Fig. 4). The relative concentration at the end part of BTCs did not reach the background value which indicates that the attachment of particles to the sand was reversible

even before injecting DI-water to the column. Therefore, a detachment coefficient (k_{det}) was considered in the modeling of these results. For experiments E1 to E7, k_{det}, α, and S_{max} were fitted to the observed breakthrough curves. The best fitted parameters with minimum RMSE are given by Table 2. Comparing the simulated parameters of all experiments revealed that the S_{max} and attachment efficiency values increased with increasing ionic strength (Fig 6).

4. Discussion

The experimental results showed that retention of MWCNTs and C_{60} nanoparticles was enhanced by increasing the ionic strength of the solution, which has also been observed in previous studies (Brant et al., 2005; Tian et al., 2012; Zhang et al., 2012; Sharma et al., 2014). On the other hand, it was observed that cylindrical shaped MWCNTs were 30% more mobile than spherical shaped C_{60} nanoparticles at high ionic strength (60 mM) while at lower ionic strength they had shown similar behavior. This means that the interaction force between nanoparticles and sand surface was in same order for both nanoparticles at low ionic strength however other mechanisms (such as aggregation, primary minima deposition, or straining due to large aggregates) are operative at higher ionic strength (Yang et al., 2013). Based on DLVO theory, increasing ionic strength reduces the size of the electrostatic double layer and repulsive forces (Hotze et al., 2010) which leads to higher retention of nanoparticles in the media at high ionic strength. Previous research has revealed that both E_v and E_{edl} forces are affected by change in the shape of nanoparticles (Vold, 1954; Bhattacharjee and Elimelech, 1997; Montgomery et al., 2000) which is consistent with our observations. Remobilization (phase III) results demonstrated that secondary minimum attachment between nanoparticles and porous media is more favorable for spherical C_{60} nanoparticles than for cylindrical MWCNTs at ionic strength of 60 mM. Some other mechanisms than secondary energy minimum attachment may also be operative which led to irreversible attachment of C_{60} nanoparticles to the sand (Fig 2b). This mechanism could be straining or aggregation in soil

295 pores but cannot be confirmed based on the current study. Theoretically straining can happen
296 when the ratio of particle diameter to sand diameter is greater than 0.003 (Bradford et al.,
297 2002). This ratio, based on the length of MWCNTs is 0.0038 but it is 0.000076 if MWCNT's
298 diameter is being used, and it is 0.00049 for C_{60} nanoparticles. The ratios are below the
299 critical ratio based on previous literature (even by using MWCNT length), which means the
300 straining is not likely an operative mechanism in these cases (Bradford et al., 2002; Jaisi et
301 al., 2008). But the stability of particles in solution at high ionic strength was critical in this
302 study. It was observed that the MWCNT solution was stable for several days even for 60 mM
303 of ionic strength. However, C_{60} solutions at ionic strengths 10.89 and 60 mM were semi-
304 stable in long-term and aggregated C_{60} particles were observed in the bottles after few hours
305 of their preparation. For larger aggregates which can ultimately increase the particle size,
306 straining and gravitational sedimentation will become more effective mechanisms for the
307 retention of particles. Therefore gravitational sedimentation is a possible mechanism that
308 would cause irreversible retention of C_{60} particles.

309 FBPs were highly mobile for the conditions of this study and only 10% of the
310 particles were retained, mostly irreversibly, in the sand column. Higher mobility of FBPs in
311 comparison with the engineered nanoparticles can be due to their stability and interaction
312 with the medium at chosen chemical and physical condition. Therefore it is not certain that
313 the shape of the FBPs has influenced their mobility and a systematic study FBP at various
314 chemical and physical conditions is needed to understand their transport scenarios in soil and
315 groundwater.

316 The modeling results suggest that S_{max} increased with increasing ionic strength, which
317 means that the site-blocking mechanism became more operative. This was probably due to
318 lowering of the repulsive energy between sand and nanoparticles at higher ionic strength and
319 an associated increase in particle attachment at primary and secondary energy minima. At

ionic strength of 1.34 mM, the value of S_{max} was greater for MWCNT than that of C_{60}, but the value of S_{max} became larger for C_{60} than MWCNTs at higher ionic strength. Increasing ionic strength is related to increasing S_{max} and α, for both C_{60} and MWCNTs in these experiments, which has also been observed in previous studies (Zhang et al. 2012). This trend indicated that increasing ionic strength results in greater attachment rate and more attachment sites, irrespective of the shape of the nanoparticles.

5. Conclusions

The aim of this study was to compare transport behavior of two types of engineered carbon-based nanoparticles (MWCNTs and C_{60}) and natural fire-born particles (FBPs) in saturated porous media. Several column experiments were conducted at a neutral pH and pore-water velocity of 7.5 m/d but the ionic strength was varied from 1.34 mM to 60 mM in order to examine the effect of ionic strength on transport of MWCNTs and C_{60} in different chemical environment.

From the experimental results of two types of carbon-based nanoparticles (C_{60} and MWCNT), it was observed that at low ionic strength (1.34 and 10.89 mM), C_{60} was relatively more mobile than MWCNTs. While at high ionic strength, the mobility of MWCNTs was much higher than that of C_{60} particles. About 50% of the retained C_{60} particles in the column were not remobilized after injecting of DI water. This suggests that irreversible attachment between the nanoparticles and sand grains became more important at higher ionic strength. Straining and gravitational sedimentation are two possible mechanisms which may have been enhanced due to formation of larger aggregates of C_{60} nanoparticles at high ionic strength and FBPs had higher mobility than engineered nanoparticles. Although the shape of nanoparticles is critical for their transport in subsurface systems, it was rather difficult to establish a quantitative relationship of transport behavior of MWCNTs and C_{60} to their shape of the nanoparticles as the background chemistry play an important role in their mobility. However,

345 the results of this study suggest that MWCNTs, C_{60} and also FBPs are highly mobile in sandy
346 saturated environments. Therefore the risk of their transport to a greater depth and
347 contamination of aquifers is considerable even at normally unfavorable conditions for particle
348 transport, such as high ionic strength in the groundwater

References

Arbuckle, W.B., Ho, Y.F. 1990. Adsorber Column Diameter: Particle Diameter Ratio Requirements. Research Journal of the Water Pollution Control Federation 62, 88-90.

Bhattacharjee, S., Elimelech, M., 1997. Surface Element Integration: A novel technique for evaluation of DLVO interaction between a particle and a flat plate. J. Colloid Interface Sci. 193, 273–285.

Bradford, S.A., Yates, S.R., Bettahar, M., Simunek, J., 2002. Physical factors affecting the transport and fate of colloids in saturated porous media. Water Resour. Res. 38, 1327, doi:10.1029/2002WR001340.

Brant, J.A., Lecoanet, H., Wiesner, M.R., 2005. Aggregation and deposition characteristics of fullerene nanoparticles in aqueous systems. J. Nanoparticle Res. 7, 545–553.

Brant, J.A., Labille, J., Bottero, J.-Y., Wiesner, M.R., 2006. Characterizing the impact of preparation method on fullerene cluster structure and chemistry. Langmuir 22, 3878–3885.

Chen, K.L., Elimelech, M., 2006. Aggregation and deposition kinetics of fullerene (C60) nanoparticles. Langmuir 22, 10994–11001.

Grassian, V.H., 2008. Nanoscience and Nanotechnology: Environmental and Health Impacts. John Wiley & Sons.

Gregory, J., 1981. Approximate expressions for retarded van der waals interaction. J. Colloid Interface Sci. 83, 138–145.

He, H., Pham-Huy, L.A., Dramou, P., Xiao, D., Zuo, P., Pham-Huy, C. 2013. Carbon Nanotubes: Applications in Pharmacy and Medicine, BioMed Res. Int. 2013, e578290. doi:10.1155/2013/578290.

Hertzberg, T. and Blomqvist, P., 2003. Particles from fire - a screening of common materials found in buildings. Fire and Materials, 27, 295-314.

374 Hotze, E.M., Phenrat, T., Lowry, G.V., 2010. Nanoparticle aggregation: challenges to
375 understanding transport and reactivity in the environment. J. Environ. Qual. 39, 1909–
376 1924.
377 Hyung, H., Fortner, J.D., Hughes, J.B., Kim, J.-H., 2007. Natural organic matter stabilizes
378 carbon nanotubes in the aqueous phase. Environ. Sci. Technol. 41, 179–184.
379 Jaisi, D. P., Saleh, N. B., Blake, R. E., Elimelech, M. 2008. Transport of single-walled carbon
380 nanotubes in porous media: Filtration mechanisms and reversibility. Environ. Sci.
381 Technol. 42, 8317–8323.
382 Jiang, J., Oberdörster, G., Biswas, P., 2009. Characterization of size, surface charge, and
383 agglomeration state of nanoparticle dispersions for toxicological studies. J.
384 Nanoparticle Res. 11, 77–89.
385 Kasel D, Bradford SA, Simunek J, Heggen M, Vereecken H, Klumpp E. 2013. Transport and
386 retention of multi-walled carbon nanotubes in saturated porous media: Effects of input
387 concentration and grain size. Water Res. 47, 913–944.
388 Klaine, S.J., Alvarez, P.J.J., Batley, G.E., Fernandes, T.F., Handy, R.D., Lyon, D.Y.,
389 Mahendra, S., McLaughlin, M.J., Lead, J.R., 2008. Nanomaterials in the environment:
390 behavior, fate, bioavailability, and effects. Environ. Toxicol. Chem. SETAC 27,
391 1825–1851.
392 Lind, C.J., 1970. Specific conductance as a means of estimating ionic strength. U.S.
393 Geological Survey Professional Paper 700-D, D272–D280.
394 Liu, J., Rinzler, A., Dai, H., Hafner, J., Bradley, R., Boul, P., Lu, A., Iverson, T., Shelimov,
395 K., Huffman, null, Rodriguez-Macias, null, Shon, Y., Lee, T., Colbert, D., Smalley,
396 R., 1998. Fullerene pipes. Science 280, 1253–1256.
397

Liu, X., O'Carroll, D.M., Petersen, E.J., Huang, Q., Anderson, C.L., 2009. Mobility of multiwalled carbon nanotubes in porous media. Environ. Sci. Technol. 43, 8153–8158.

Mashayekhi, H., Ghosh, S., Du, P., Xing, B., 2012. Effect of natural organic matter on aggregation behavior of C60 fullerene in water. J. Colloid Interface Sci. 374, 111–117.

Mattison, N.T., O'Carroll, D.M., Kerry Rowe, R., Petersen, E.J., 2011. Impact of porous media grain size on the transport of multi-walled carbon nanotubes. Environ. Sci. Technol. 45, 9765–9775.

Mekonen, A., Sharma, P., Fagerlund, F., 2014. Transport and mobilization of multiwall carbon nanotubes in quartz sand under varying saturation. Environ. Earth Sci. 71, 3751–3760.

Montgomery, null, Franchek, null, Goldschmidt, null, 2000. Analytical Dispersion Force Calculations for Nontraditional Geometries. J. Colloid Interface Sci. 227, 567–584.

Nisbet, I.C.T., LaGoy, P.K., 1992. Toxic equivalency factors (TEFs) for polycyclic aromatic hydrocarbons (PAHs). Regul. Toxicol. Pharmacol. 16, 290–300.

O'Carroll, D.M., Liu, X., Mattison, N.T., Petersen, E.J., 2013. Impact of diameter on carbon nanotube transport in sand. J. Colloid Interface Sci. 390, 96–104.

Petersen, E.J., Zhang, L., Mattison, N.T., O'Carroll, D.M., Whelton, A.J., Uddin, N., Nguyen, T., Huang, Q., Henry, T.B., Holbrook, R.D., Chen, K.L., 2011. Potential Release Pathways, Environmental Fate, And Ecological Risks of Carbon Nanotubes. Environ. Sci. Technol. 45, 9837–9856.

Seymour, M.B., Chen, G., Su, C., Li, Y., 2013. Transport and Retention of Colloids in Porous Media: Does Shape Really Matter? Environ. Sci. Technol. 47, 8391–8398.

422 Sharma, P., Bao, D., Fagerlund, F., 2014. Deposition and mobilization of functionalized
423 multiwall carbon nanotubes in saturated porous media: effect of grain size, flow
424 velocity and solution chemistry. Environ. Earth Sci. 72, 3025–3035.
425 Sharma, P., Fagerlund, F., 2015. Transport of Surface-modified Carbon Nanotubes through a
426 Soil Column. J. Vis. Exp. 98, doi:10.3791/52634.
427 Sharma, P.; Abdou, H.; Flury, M. 2008a. Effect of the lower boundary condition and flotation
428 on colloid mobilization in unsaturated sandy sediments. Vadose Zone J. 7, 930–940.
429 Sharma, P.; Flury, M.; Zhou, J. 2008b. Detachment of colloids from a solid surface by a
430 moving air-water interface. J. Colloid Interface Sci. 326, 143–150.
431 Sharma, P., Flury, M., Mattson, E.D., 2008c. Studying colloid transport in porous media
432 using a geocentrifuge. Water Resour. Res. 44, W07407, doi:10.1029/2007WR006456.
433 Sharma P., 2012. Geological disposal of nuclear waste: Fate and transport of radioactive
434 materials, in Nuclear Power - Practical Aspects, Editor: Wael Ahmed, InTech, ISBN:
435 978-953-51-0778-1.
436 Sharma, P., Fagerlund, F., Iverfeldt, U., Eskebaek, A. 2016. Fate and transport of fire-born
437 particles in porous media. Technologies 4, 2, doi:10.3390/technologies4010002.
438 Tan, C.W., Tan, K.H., Ong, Y.T., Mohamed, A.R., Zein, S.H.S., Tan, S.H., 2012. Energy and
439 environmental applications of carbon nanotubes. Environ. Chem. Lett. 10, 265–273.
440 Tian, Y., Gao, B., Wu, L., Munoz, R., Huang, Q. 2012. Effect of solution chemistry on multi-
441 walled carbon nanotube deposition and mobilization in clean porous media. J. Hazard.
442 Mater. 231-232, 79–87.
443 Vold, M.J., 1954. Van der Waals' attraction between anisometric particles. J. Colloid Sci. 9,
444 451–459.
445 Wang, J., Chen, Y., Blau, W.J., 2009. Carbon nanotubes and nanotube composites for
446 nonlinear optical devices. J. Mater. Chem. 19, 7425–7443. doi:10.1039/B906294G

Wang, Y., Li, Y., Pennell, K.D., 2008. Influence of electrolyte species and concentration on the aggregation and transport of fullerene nanoparticles in quartz sands. Environ. Toxicol. Chem. SETAC 27, 1860–1867.

Xu, M., Eckstein, Y., 1997. Statistical analysis of the relationships between dispersivity and other physical properties of porous media. Hydrogeol. J. 5, 4–20.

Yang, Y., Nakada, N., Nakajima, R., Yasojima, M., Wang, C., Tanaka, H., 2013. pH, ionic strength and dissolved organic matter alter aggregation of fullerene C60 nanoparticles suspensions in wastewater. J. Hazard. Mater. 244–245, 582–587.

Zhang, L., Hou, L., Wang, L., Kan, A.T., Chen, W., Tomson, M.B., 2012. Transport of fullerene nanoparticles (nC60) in saturated sand and sandy soil: controlling factors and modeling. Environ. Sci. Technol. 46, 7230–7238.

Zhang, L., Zhang, Y., Lin, X., Yang, K., Lin, D., 2014. The role of humic acid in stabilizing fullerene (C60) suspensions. J. Zhejiang Univ. Sci. 15, 634–642.

460 **List of figures and tables**

461 **Figure 1:** Observed breakthrough curves for C_{60} (E1, E2, and E3) and MWCNTs (E4, E5,
462 and E6) at different ionic strengths (phase I, II and III). The solid points represent the
463 experimental data and solid lines represent the results of simulations for phase I and II.

464 **Figure 2:** Proportion of the outflow C_{60} or MWCNTs nanoparticles to total input
465 concentration during (a) phase 1 and 2, (b) phase 3. (The values are the average of three
466 replication of the experiments±standard deviation.)

467 **Figure 3:** Comparison of observed BTCs for MWCNTs, C_{60} and FBPs at pH of 7 and ionic
468 strength of 60 mM, experimental data are shown in points with their corresponding
469 simulations in lines.

470 **Figure 4:** Scanning electron microscopy images of filtered (< 11 μm size) samples (a) inflow
471 for column experiments and (b) exited from column experiments.

472 **Figure 5:** DLVO energy profiles at different ionic strength for (a) C_{60} and (b) MWCNTs with
473 effective diameter for MWCNTs based as its hydrodynamic diameter obtained from particle
474 size analysis.

475 **Figure 6:** Relationship of ionic strength with modeling parameter (a) attachment efficiency
476 and (b) S_{max} for MWCNTs and C_{60}

477

478 **Table 1:** Properties during column experiments

479 **Table 2:** Experimental conditions, model fitted parameters and their root-mean square error.

480 **Table 3:** Parameters used for DLVO calculations

Figure 1

Click here to download Figure Fig. 1.tif

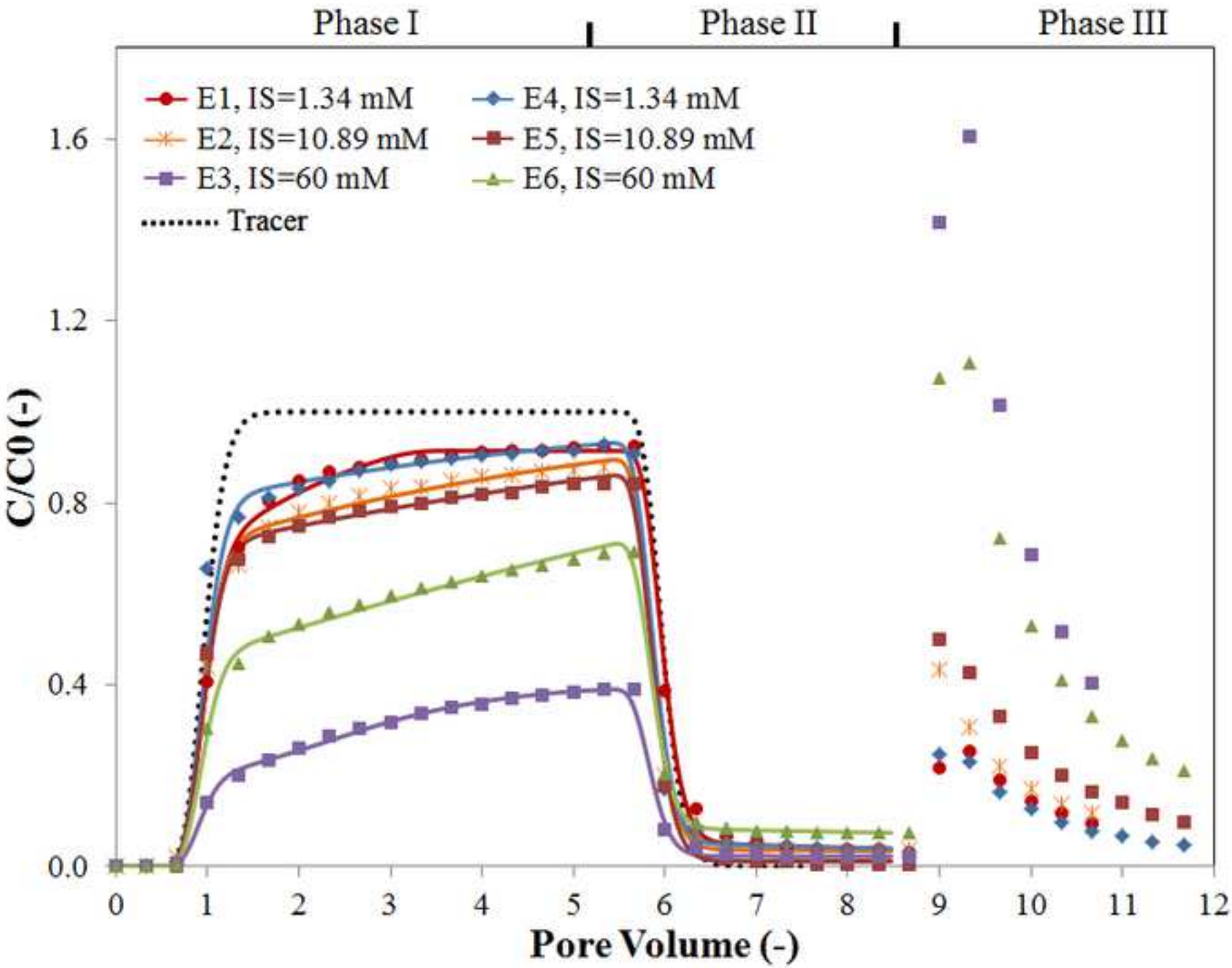

Figure 2

Click here to download Figure Fig. 2.tif

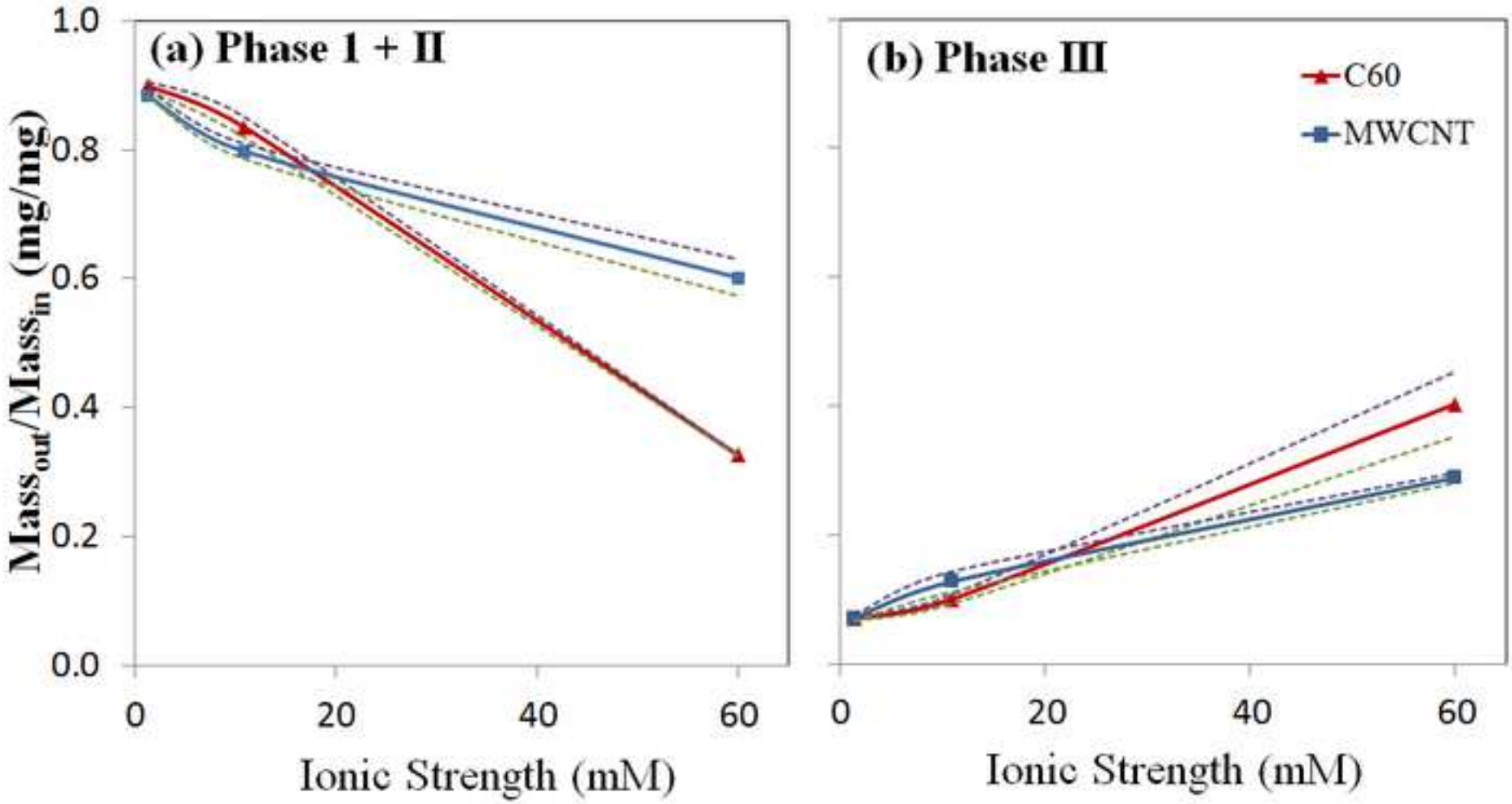

Figure 3

Click here to download Figure Fig. 3.tif

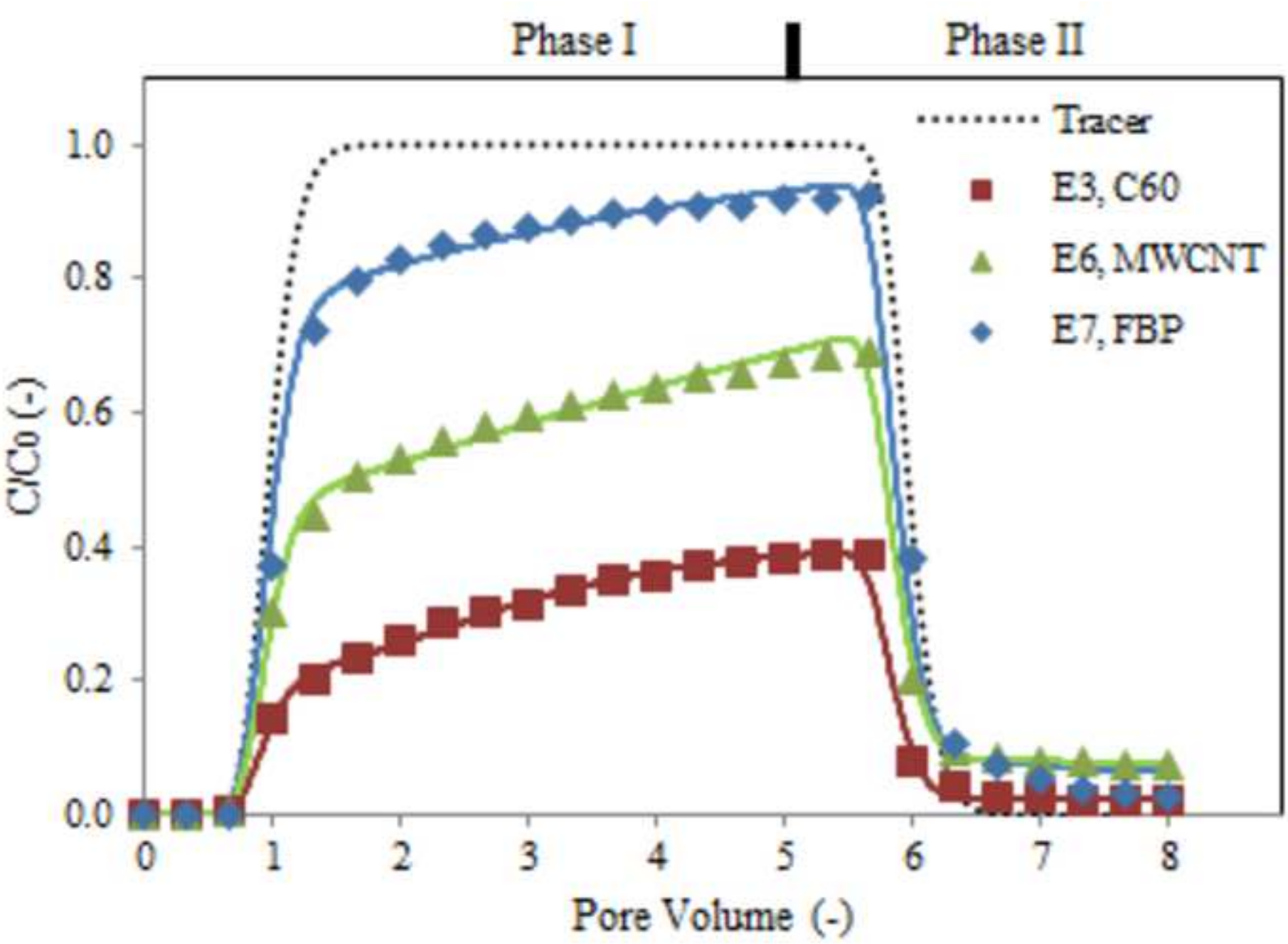

Figure 4

Click here to download Figure Fig. 4.tif

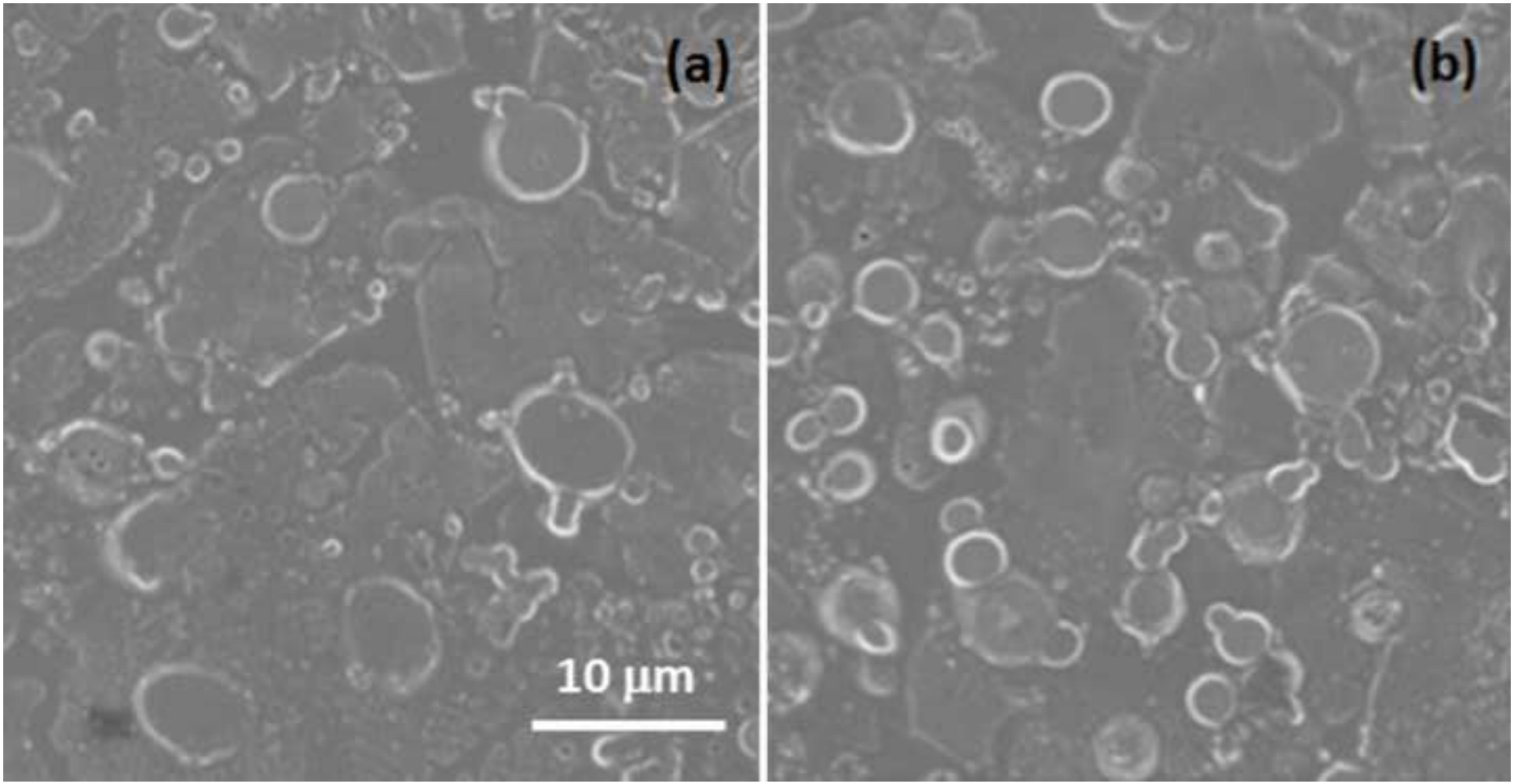

Figure 5

Click here to download Figure Fig. 6.tif

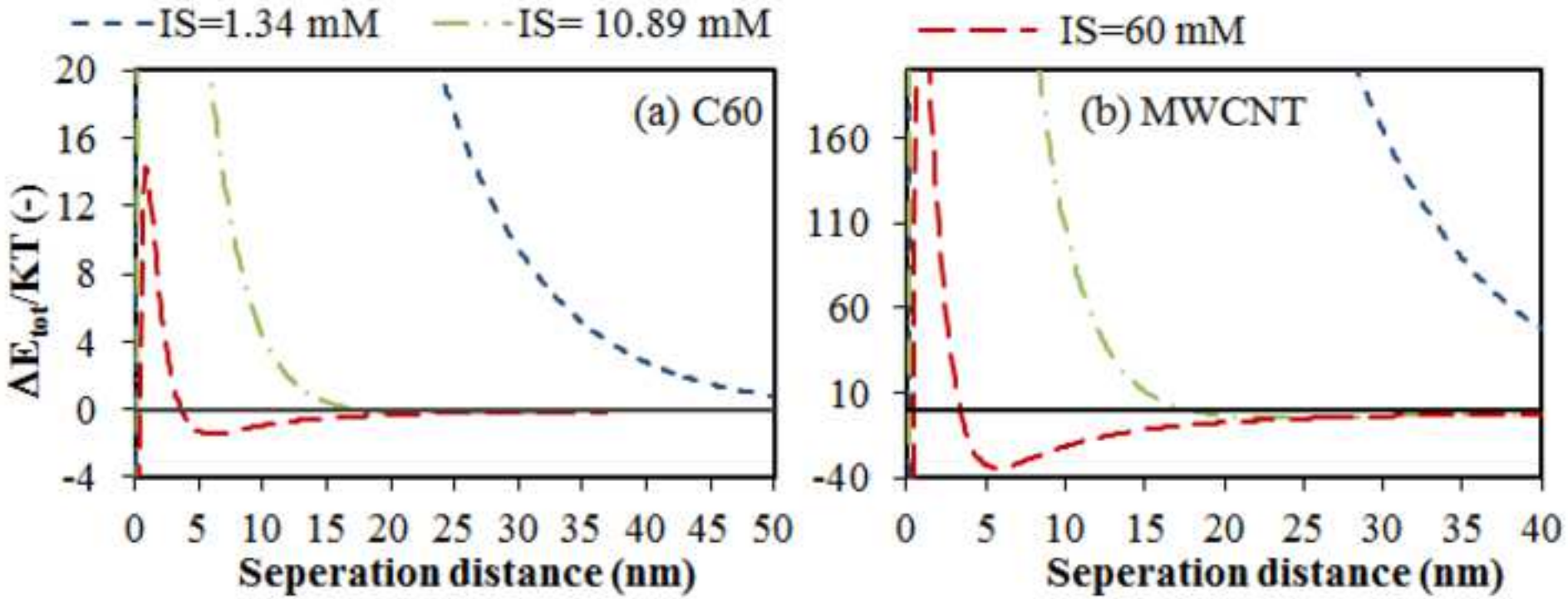

Figure 6

Click here to download Figure Fig. 7.tif

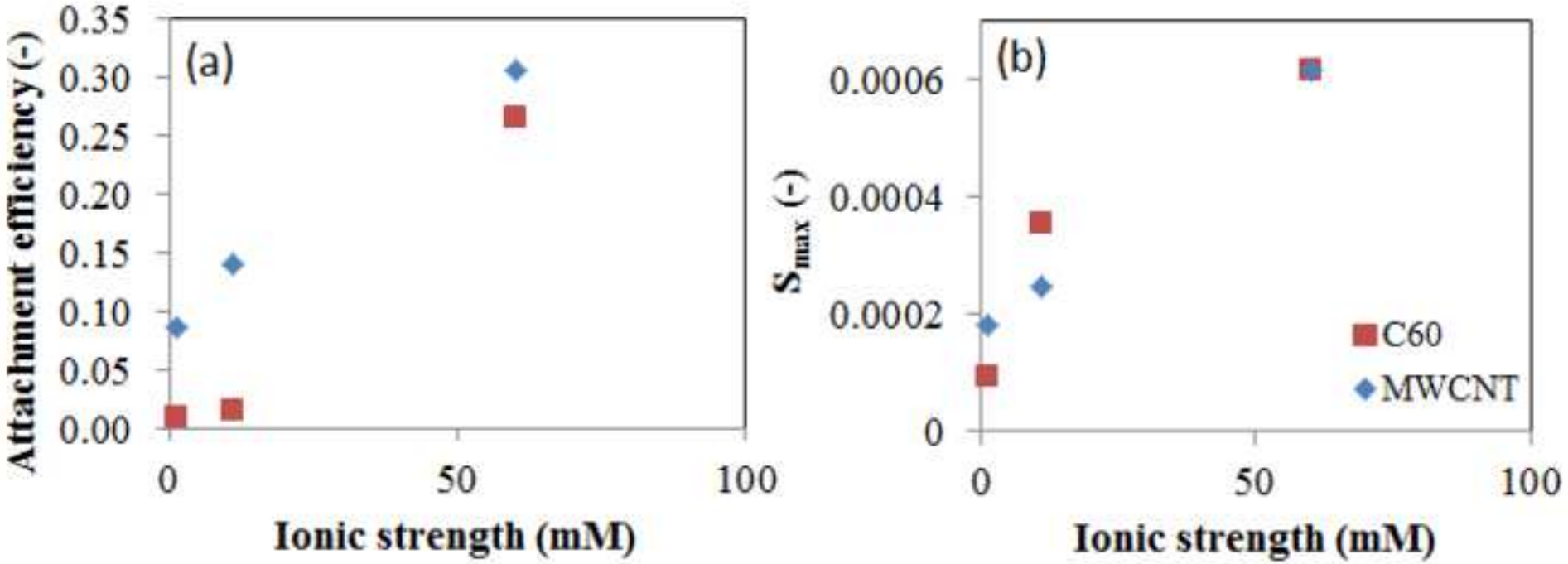

table Click here to download table Table .docx

Table 1: Properties during column experiments

Grain size	250-450 μg
Weight of sand	120 g
Bulk density	1.63 g/cm^3
Porosity	0.39
Saturated pore volume	28.35 ml
Temperature	21-22˚C
Pore water velocity	7.5 m/d

Table 2: Experimental conditions, model fitted parameters and their RMSE

Experiment	Particle	IS (mM)	α	S_{max}	K_{det}	α_1 (m)	RMSE
E1	C60	1.34	9.15×10^{-3}	9.41×10^{-5}	3.42×10^{-5}	2.60×10^{-3}	0.061
E2	C60	10.89	1.47×10^{-2}	3.51×10^{-4}	1.10×10^{-5}	2.60×10^{-3}	0.083
E3	C60	60	2.66×10^{-1}	6.30×10^{-4}	3.33×10^{-6}	2.60×10^{-3}	0.021
E4	MWCNT	1.34	8.71×10^{-2}	1.80×10^{-4}	2.20×10^{-5}	2.60×10^{-3}	0.268
E5	MWCNT	10.89	1.41×10^{-1}	2.47×10^{-4}	3.06×10^{-6}	2.60×10^{-3}	0.072
E6	MWCNT	60	3.06×10^{-1}	6.13×10^{-4}	1.26×10^{-5}	2.60×10^{-3}	0.060
E7	FBP	61.12	8.79×10^{-2}	3.15×10^{-4}	3.45×10^{-5}	2.60×10^{-3}	0.302

Table 3: Parameters used for DLVO calculations

Particle	Hydrodynamic diameter of NPs (nm)[a]	Zeta potential of NPs (mV)	Ionic strength (mM)	Zeta potential of sand (mV)[c]	Hamaker constant (J)[d]
C_{60}	618.9	-40	1.34	-57.3	6.7×10^{-21}
C_{60}	644.5	-39	10.89	-43.2	6.7×10^{-21}
C_{60}	701.2	-15	60	-29.1	6.7×10^{-21}
MWCNT	106.7	-41.7	1.34	-57.3	9.8×10^{-21}
MWCNT	111	-34.7	10.89	-43.2	9.8×10^{-21}
MWCNT	141.2	-19.6	60	-29.1	9.8×10^{-21}
FBP	360	-5	60[b]	-29.1	3.84×10^{-21}

[a]Diameter measured using zeta-sizer. [b]Converted from measured electrical conductivity. [c]Zeta potential of sand was obtained using surface analyzer. [d]Hamaker constant estimated from literature.